Observation of turbulence energy transfer in a cylindrical laboratory plasma

J.T.Ma, W.W.Xiao*, C.Y.Wang, W.J.Zhong, and Wali Niaz
Institute for Fusion Theory and Simulation, School of Physics, Zhejiang University, Hangzhou, 310027, China

(*Author to whom correspondence should be addressed:wwxiao@zju.edu.cn)

(Dated: 8 April 2023)

We report the experimental results on the turbulence energy transfer in a cylindrical laboratory plasma based on the data obtained by a set of Quadruple Langmuir Probe (QLP) on Zheda Plasma Experiment Device (ZPED). The turbulence energy transfer is directly embodied in the alternating change of the fluctuation amplitudes between the low frequency shear flow (LFSF) at $\sim 0.2kHz$ and the drift wave (DW) turbulence at $\sim 1-2kHz$. The estimation of radial electric field and bispectral analysis of the experiments suggest that the DW turbulence gains the energy from the low frequency turbulence. The energy transport due to the interaction between the LFSF ant the DW turbulence with the magnetic field increase is a possible reason to drive the turbulence energy transfer in the laboratory plasma.

Keywords: turbulence energy transfer, low frequency shear flow, drift wave turbulence, energy transport

I. INTRODUCTION

Turbulence affects the confinement of the magnetized plasma is a fundamental plasma physics. The confinement of particle and energy is controlled by the competition and the nonlinear energy transport between the high frequency turbulence and the LFSF have been studied in tokamak plasmas[1–5]. In the cylindrical laboratory plasma devices, such as CSDX[6–13], LMD/LMD-U[14–17], PANTA[14], were designed for the studies of the basic physical processes of the turbulence. Drift wave-shear flow system has also been observed in linear plasma devices[7–9,14,18,19] and the nonlinear energy transport between $\mathbf{E}\times\mathbf{B}$ shear flow and drift wave (DW) turbulence were studied by evaluating Reynolds stress and bispectral analysis[7,9,10,17]. Experiments show that with the magnetic field B rising, the density gradient deepens and a transport barrier forms at a critical value in the cylindrical laboratory plasmas[13,14]. Reduced fluid models are also developed on CSDX[20,21] and PANTA[22–25] to describe and simulate the dynamics of drift wave-shear flow system. A physical process of the decoupling-coupling-decoupling (DCD) regime of the electron density (n_e) and temperature (T_e) in the ZPED[26] was observed and studied[27]. The previous studies show that many laboratory plasma experiments have been conducted for the basic physics of drift-wave turbulence.

We report the experimental results on the turbulence energy transfer in the ZPED based on the estimation of radial electric field and the bispectral analysis from the data obtained by a set of Quadruple Langmuir probe. By comparing the radial turbulence structure and the radial electric field, we deliver a further understanding of the turbulence energy transfer, which is directly indicated in the alternating change of the fluctuation amplitudes between the low frequency shear flow (LFSF) at $0.2kHz$ and the drift wave turbulence at $1-2kHz$. The bispectral analysis is used to detect whether there is phase coupling occurring in fluctuation. The experimental results suggest that the energy evolution of the turbulence system, including the proportion of energy transport and the turbulence radial structure associated with radial electric field (E_r), is still required to furtherly study to refine the understanding of the confinement and transport in the plasma physics.

The paper is organized as follows: The experimental conditions are described in section II. The data analysis methods are introduced in section III. The experimental results, including the measurement results of the density and the temperature, the understanding of turbulence energy transfer, are given in section IV. Section V is the summary and discussion.

II. EXPERIMENTAL CONDITIONS

ZPED is a cylindrical magnetized plasma device at Zhejiang University, with a vacuum chamber of $2.0m$ long and $0.3m$ in diameter. The Nitrogen plasma column used for experiments is produced by a $13.56MHz$ $200W$ radio frequency (RF) source with a radius of approximately $9cm$ (z: axial, r: radial, θ: poloidal direction).

The Quadruple Langmuir probe (QLP)[26] placed perpendicular to the magnetic field and movable in the radial direction is the major diagnostic tool of the experiments. The four tips of the QLP are of $2.5mm$ in length and $0.4mm$ in diameter. The distance of the poloidal pair of tips (Δd) is $5mm$. Both the radial profiles of electron density n_e and temperature T_e and four signals of floating potentials are measured by the QLP with different circuits. The sampling frequency of the experimental data is the $2MHz$ acquisition device. The details of experimental conditions of the ZPED were reported in[26,27]. In this work, all plasma discharges were performed in the ZPED.

III. ANALYSIS METHOD OF THE EXPERIMENTAL DATA

A. Estimation of radial electric field

Langmuir probes to measure the floating potential V_f had been pointed out by P. Stangeby and G. McCracken[28] [28]. The relation for potential drop across the sheath V_{sf} for floating conditions is $V_{sf}\equiv V_f - V_p$ as V_p being the plasma potential at the sheath edge. Considering the secondary electron

emission coefficient δ, one can derive the potential drop as (see Stangeby [29] for the detailed derivation):

$$V_{sf} = \frac{kT_e}{2e} \ln \left[2\pi \frac{m_e}{m_i} \left(1 + \frac{T_i}{T_e} \right) (1-\delta)^{-2} \right] \quad (1)$$

For the Nitrogen plasma in ZPED, the typical electron temperature is $T_e \sim 5eV$ and assumed $T_e \gg T_i$, with $\delta = 0$, we can obtain:

$$V_{sf} = -4.16kT_e/e, \quad V_p = V_f + 4.16kT_e/e \quad (2)$$

The local electric field can then be calculated as $\mathbf{E}_r = -\nabla_r V_p$.

B. Bispectral analysis

To study the nonlinear interaction among the fluctuation signals $\tilde{\phi}_f$, we use the bispectral analysis[30] which is widely used in both Tokamaks[31] and linear devices[6,9,14,17] to detect the phase coupling that occurs between the signals. As pointed out by Yong C. Kim and Edward J. Powers[30], the determination of the coupling coefficient is important as the physics of nonlinear wave coupling is binded on the coupling efficient. Follow the definition of the power spectrum as the second-order cumulant spectra $P(f) = E[X_f X_f^*]$, the bispectrum is defined as the third-order cumulant as $X(f)$ is the Fourier component of the fluctuation signal $x(t)$:

$$B(f_1, f_2) = E[X(f_1)X(f_2)X^*(f_1+f_2)] \quad (3)$$

The definition shows that the bispectrum $B(f_1, f_2)$ measures the statical dependence between three waves[32]. With the symmetry relations of the bispectrum:

$$B(f_1, f_2) = B(f_2, f_2) = B^*(-f_1, -f_2) \quad (4)$$
$$B(f_1, f_2) = B(-f_1 - f_2, f_2) = B(f_1, -f_1 - f_2) \quad (5)$$

we only need the primary zone of the $f_1 - f_2$ plane ($f_1 \geqslant f_2, f_1 \leqslant -f_2$ and $f_1 \geqslant 0$) to study the coupling behavior.

To determine the degree of interaction among three waves, we use the bicoherence spectrum $b(f_1, f_2)$:

$$b^2(f_1, f_2) = \frac{|B(f_1, f_2)|^2}{E[|X(f_1)X(f_2)|^2]E[|X(f)|^2]} \quad (6)$$

where $f = f_1 + f_2$. As the bicoherence $b(f_1, f_2)$ is defined as the normalization of bispectrum by auto and cross power spectrum, the value of bicoherence is limited to $0 \leqslant b \leqslant 1$, and the value close to unity indicate the wave interaction has occurred between the waves. Since the quantity $b^2(f_1, f_2)P(f)$ indicates the power of wave at f due to wave-wave interaction at f_1 and f_2, $b^2(f_1, f_2)$ measures the ratio of power at f due to the wave-wave interaction to the whole power at f.

IV. EXPERIMENTAL RESULTS

A. Profiles of the n_e and T_e and the gradient length evolutions of the n_e and T_e

To obtain the radial profiles of the n_e and T_e in the ZPED, the QLP is swept radially from edge to center while continuously data-collecting. The results of the radial profiles of electron density n_e and electron temperature T_e with different magnetic fields are shown in Figure 1, respectively. Here, (a) is the density profiles, (b) is the temperature profiles and the r refers to the radial positions. In our experiments, we chose a key region of analysis at $r \sim 3.4cm$ (as shown by the black dashed lines in figure 1) because of the diagnostic error of the probes in the edge and center of laboratory plasmas[26].

The gradient length of both density ($1/L_{n_e} = |\nabla_r n_e|/n_e$) and temperature ($1/L_{T_e} = |\nabla_r T_e|/T_e$)[33] are calculated based on the profiles of the density and the temperature as shown in figure 1. The details are shown in Figure 2, with the blue curve and the red curve representing the density and temperature gradient length respectively.

Here, in region I, with the magnetic field rising from $\sim 500Gs$ to $\sim 800Gs$, the plasma begins to be contained, so that the density gradient increases intensely, while the temperature gradient decreases slightly. When the magnetic field rising from $\sim 800Gs$ to $\sim 1250Gs$ in region II, the density gradient and the temperature gradient increase synergistically. In region III, with the magnetic field rising above $\sim 1250Gs$ to $\sim 1700Gs$, the density gradient keep increases while the temperature gradient appears to be opposite. This indicates that the density gradient and the temperature gradient are first decoupled in region I, then coupled in region II and decoupled again in region III, which are in evidently agreement with previous work[26]. The turbulence measurement and analysis in different magnetic fields are presented in this section IV B and IV C.

B. Evolutions of the turbulence amplitudes with different magnetic fields

The power spectrum of the floating potential fluctuations $\tilde{\phi}_f$ in different magnetic fields according to Fig. 2 are calculated as shown in Fig. 3. An evolution progress of the turbulence amplitudes with different magnetic fields was observed. When the magnetic field first starts to rise, the turbulence is not fully developed as shown in figure 3 (a). Then, a coexistence of two fluctuations with different frequencies is observed, a low frequency around $f_1 \sim 0.2kHz$ and a high frequency of $f_2 \sim 1-2kHz$, as shown in figure 3 by the black and the red arrows, respectively. Especially, the turbulence amplitude of f_2 rises while that of f_1 drops with the increasing of magnetic field as shown in the figure 3 from the (b) to the (c). This indicates the turbulence energy accumulates at f_2 and damps at f_1. It means that there is a turbulence energy transfer which is directly embodied by the alternating change of the turbulence amplitude between the low frequency turbulence at $\sim 0.2kHz$ and the high frequency turbulence at $\sim 1-2kHz$. When the magnetic field continuously increases, a broadband turbulent burst is observed from $\sim 0.1kHz$ to $\sim 20kHz$, as shown in figure 3 (d).

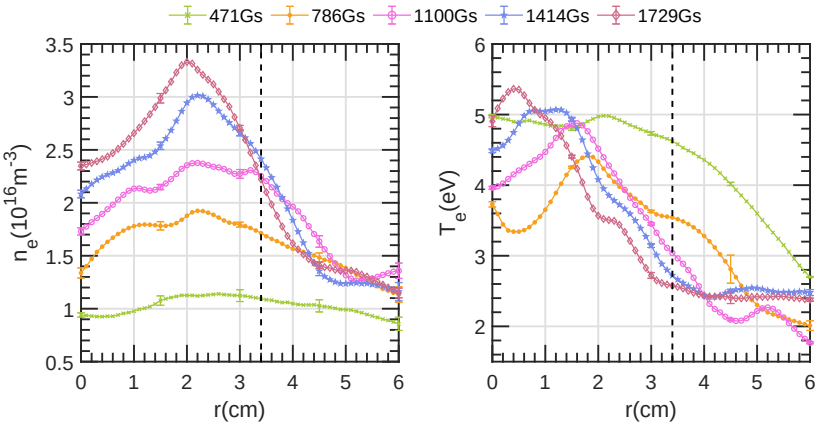

FIG. 1. Radial profiles of the density and the temperature with different magnetic fields in ZPED. The key region of analysis is at $r = 3.4cm$ as shown by the black dashed lines.

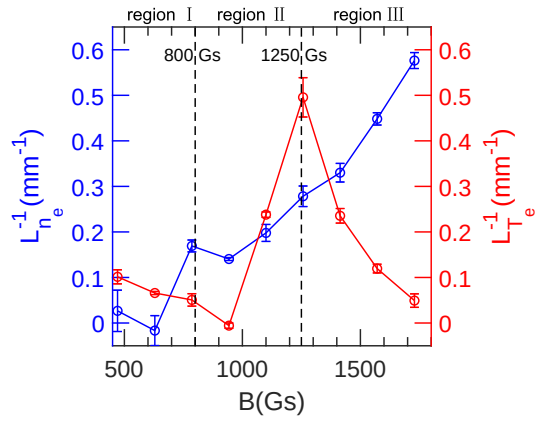

FIG. 2. The evolution of the $1/L_{n_e}$ and $1/L_{T_e}$ at $r = 3.4cm$ with the increasing of magnetic field. The different magnetic fields are defined with three regions, I, II and III.

C. The formation and damping of the LFSF during DCD

In order to understand the characteristics of the turbulence energy transfer, we analyzed the radial power spectrum and the radial electric field E_r, which can be calculated by equation 2. The relationship between the radial turbulence structures and the radial electric field E_r is analyzed in different magnetic fields.

First, the radial auto-power spectrum in different magnetic fields is presented in figure 4(a)-(e). Meanwhile, the results of the radial electric fields E_r are calculated as shown in figure 4(f)-(j). The color bar means the turbulence amplitude of the floating potential fluctuations $\tilde{\phi}_f$. It is clear that there is a shear layer at r $1.8-4cm$. Here, the E_r in the other regions exists different amplitudes and distributions, as shown in figure 4 (f)-(j). This shear layer along the radial direction in the plasma is marked in figure 4 by the shaded bars. This indicates that a low frequency shear flow (LFSF) exists in this region from r $1.8-4cm$ due to the poloidal rotation induced by the E_r.

Two frames of the radial auto-power spectrum and the E_r are specially highlighted by the red dashed box to show a competitive behavior between the poloidal rotation induced by the E_r and the radial structure of the turbulence at $\sim 1-2kHz$. Obviously, when the magnetic field reaches around $943Gs$, the turbulence of $\sim 1-2kHz$ is formed and has a radial structure at the location of $r \sim 1.8-4cm$, as shown in figure 4(b). While, with the magnetic field continuous increasing, the radial structure of the turbulence is stretched and torn up exactly due to the stronger E_r effect, as shown in figure 4(g) and (h). And, when the magnetic field reaches above $1250Gs$, the shearing effect weakened which results in a radially regathering of the turbulence at $\sim 1-2kHz$. These results are strongly consistent with the power spectral density (PSD) of floating potentials as shown in figure 3(b) and (c). Meanwhile, the color change of the radial turbulence structures also suggests that the turbulence amplitudes were modulated by the poloidal shear increasing. Thus, the experimental results show that the interaction of the shear flow and the radial turbulence could be the driven source of the turbulence amplitude change. And the direction of the turbulence energy transfer is inferred that the DW turbulence with the frequency at $\sim 1-2kHz$ gains the energy from the low frequency turbulence at $\sim 0.2kHz$ when the magnetic field increasing.

D. Energy transport between the LFSF and the DW turbulence

An energy transport between the LFSF ($\sim 0.2kHz$) and the DW turbulence ($\sim 1-2kHz$) is also examined by the bispectrum (Equation 3) and the auto-bicoherence (Equation 6). The results are showing in figure 5 and figure 6.

The value of $B(f_1, f_2)$ at $f = f_1 + f_2$ is higher than that of other frequencies, As shown in figure 5(b) and (c). Furthermore, the value of $b^2(f_1, f_2)$ at the same frequency corresponding to the figure 6(c) reaches an average value of 0.4 with a maximum of 0.6, as showing in figure 6(b). Since the

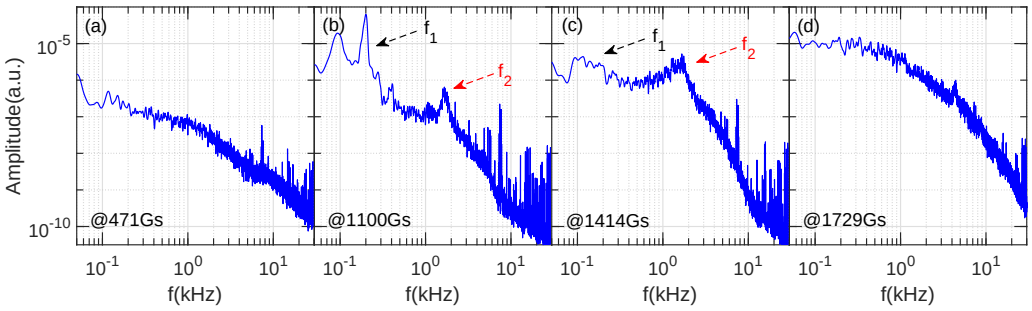

FIG. 3. Evolution progress of the turbulence amplitudes using by the power spectral density (PSD) at $r \sim 3.4cm$ with different magnetic fields. The turbulence energy transfer exists with the magnetic field increase. The low frequency turbulence and the high frequency turbulence are noted by the black ($\sim 0.2kHz$) and the red arrows ($\sim 1-2kHz$), respectively.

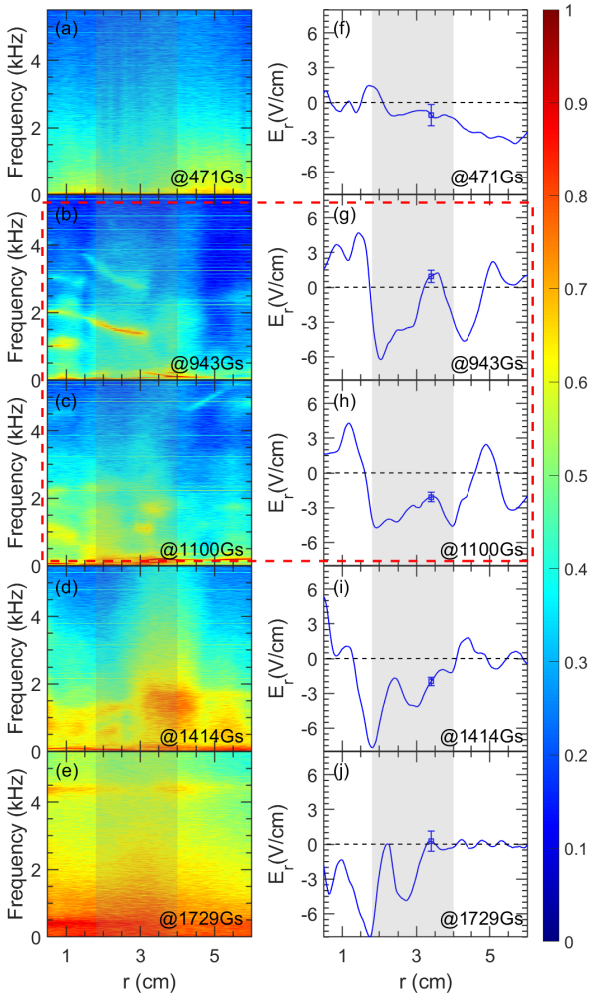

FIG. 4. The radial distributions of the power spectra (a)-(e) and the radial electric field E_r (f)-(j). The shear layer of $r \sim 1.8-4cm$ is indicated with the shaded bars. The red dashed box represents the competitive behavior between the radial turbulence structure and shear effect. The color bar represents the fluctuation amplitude of the floating potential fluctuations $\tilde{\phi}_f$.

energy of the LFSF achieves its peak as shown in figure 3(b) and damps as shown in figure 3(c), which synchronized with the phenomenon of the turbulence energy transport based on the intensity of the wave-wave interaction, we assume it can only gain energy from nonlinear interaction between the turbulence at f_1, f_2 and damp due to collision[34]. Especially, the comparison between figure 5 and figure 6 indicates a relatively strong interaction of the f_1 and the f_2 exists in figure 5(b) and in figure 6(b). Note: a possibility of the unclear proportion of energy in figure 6(c) and (d) is from the comprehensive burst of turbulence with the magnetic field increase, as shown in figure 3(c) and (d) and figure 4(d) and (e). This means there is a coexistence status accompanied by competitive relationships between the LFSF and the DW turbulence, until this coexistence status is broken due to the magnetic field increasing. This suggests the energy transport due to the wave-wave interaction between the turbulences at f_1, $f_2$is a possible driven source of the turbulence energy transfer.

V. SUMMARY AND DISCUSSION

Experimental results on the turbulence energy transfer in the ZPED has been studied based on the profiles measurements, the evolutions of the turbulence amplitudes and the bispectral analysis method in different magnetic fields. Based on the power spectral density (PSD) of floating potentials, the turbulence energy transfer is directly embodied in the alternating change of the fluctuation amplitudes with different magnetic fields.

By comparing the turbulence radial structure and the radial electric field, the understanding of the turbulence energy transfer between the low frequency shear flow (LFSF) at $\sim 0.2kHz$ and the DW turbulence at $\sim 1-2kHz$ could be delivered since the radial structure of the turbulence is stretched and torn up exactly due to the stronger E_r effect. The DW gains the energy from the low frequency turbulence at $\sim 0.2kHz$ when the magnetic field increasing. Clearly, the turbulence amplitude change indicated by the color bar as shown in figure 4, it suggests that the interaction of the shear flow and the radial turbulence is the driven source of the turbulence

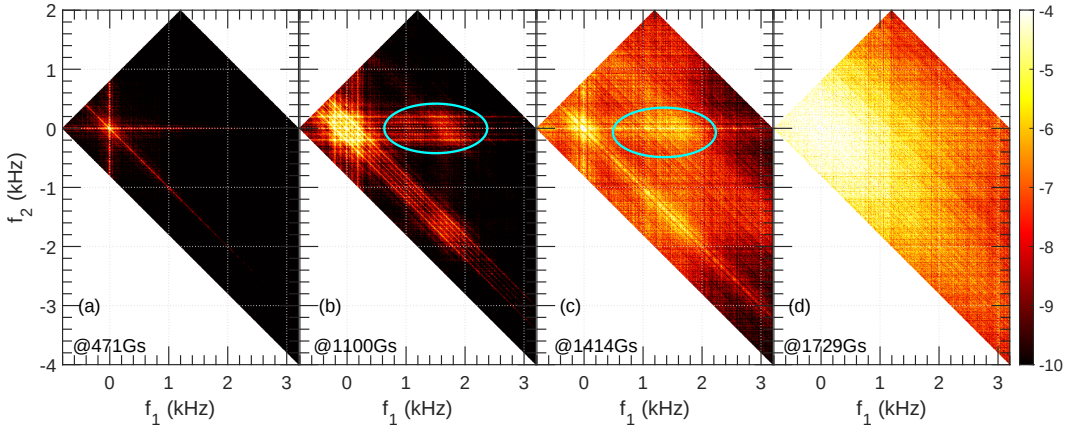

FIG. 5. Bispectrum $B(f_1, f_2)$ of floating potentials under different magnetic fields at $r = 3.4cm$. The statical dependence of $f = f_1 + f_2$ due to the nonlinear interaction of f_1 and f_2 is indicated with different colors. The cyan ellipses mark the interaction between the LFSF ($\sim 0.2kHz$) and the DW turbulence ($\sim 1-2kHz$)

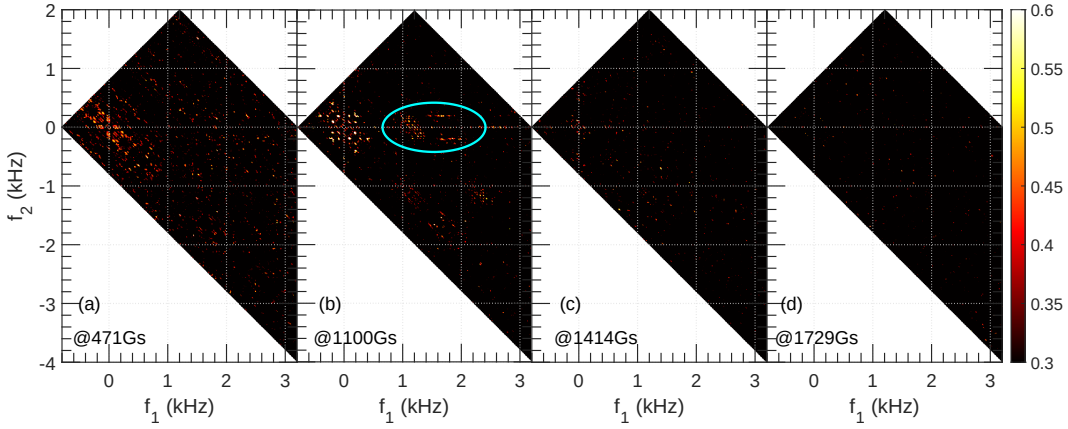

FIG. 6. Auto-bicoherence $b^2(f_1, f_2)$ of floating potentials under different magnetic fields at $r = 3.4cm$. The proportion of energy of $f = f_1 + f_2$ due to nonlinear energy transport between f_1 and f_2 is indicated with different colors. The cyan ellipse marks the location of $b2(f1, f2)0.4$, which indicates a relatively strong nonlinear interaction of the f_1 and f_2.

amplitude changes. The direction of the turbulence energy transfer is inferred that the DW turbulence with the frequency at $\sim 1-2kHz$ gains the energy from the low frequency turbulence at $\sim 0.2kHz$ when the magnetic field increasing.

Meanwhile, the comparison based on the bispectral analysis indicates a relatively strong interaction of the f_1 and the f_2 existed in a coexistence status, such as in region II, until the coexistence status was broken due to the magnetic increasing. The result of the comparison suggests that the energy transport progress between the LFSF and the DW turbulence during the magnetic field increasing is based on the intensity of the wave-wave interaction to induce the turbulence energy transfer. Here, we assume DW turbulence energy only can gain the energy from nonlinear interaction and damp due to collision. Thus, the energy transport induced by the wave-wave interaction between the turbulence at f_1, $f_2$is a possible driven source of the turbulence energy transfer. The disappearance and appearance of the turbulence of $12kHz$ and $45kHz$, such as in figure 4(e) and (j), during the transformation of the new profiles and their relation with the confinement are still unclear, which requires further study.

ACKNOWLEDGMENTS

The author (W.W. Xiao) would like to thank Dr. K.J. Zhao for the fruitful discussion. This work was supported by the National Natural Science Foundation of China (Grant No.11875234), the National Magnetic Confinement Fusion Science Program of China (2017YFE0301200, 2017YFE0301206 and 2017YFE0300500).

[1] G. R. Tynan, R. A. Moyer, M. J. Burin, and C. Holland, "On the nonlinear turbulent dynamics of shear-flow decorrelation and zonal flow generation," Physics of Plasmas **8**, 2691–2699 (2001).

[2] J. Cheng, J. Q. Dong, L. W. Yan, et al., "Roles of turbulence– and pressure-gradient–induced flows in triggering h-mode at marginal heating power on HL-2a tokamak," EPL (Europhysics Letters) **116**, 15001 (2016).

[3]P. Manz, M. Xu, N. Fedorczak, et al., "Spatial redistribution of turbulent and mean kinetic energy," Physics of Plasmas **19**, 012309 (2012).
[4]X. Wu, G. Xu, B. Wan, et al., "One-dimensional modelling of limit-cycle oscillation and h-mode power scaling," Nuclear Fusion **55**, 053029 (2015).
[5]K. Zhao, Y. Shi, H. Liu, et al., "Co-current toroidal rotation-driven and turbulent stresses with resonant magnetic perturbations in the edge plasmas of the j-text tokamak," Nuclear Fusion **56**, 076005 (2016).
[6]M. J. Burin, G. R. Tynan, G. Y. Antar, et al., "On the transition to drift turbulence in a magnetized plasma column," Physics of Plasmas **12**, 052320 (2005).
[7]C. Holland, J. H. Yu, A. James, et al., "Observation of turbulent-driven shear flow in a cylindrical laboratory plasma device," Phys. Rev. Lett. **96**, 195002 (2006).
[8]G. R. Tynan, C. Holland, J. H. Yu, et al., "Observation of turbulent-driven shear flow in a cylindrical laboratory plasma device," Plasma Physics and Controlled Fusion **48**, S51 (2006).
[9]Z. Yan, G. R. Tynan, C. Holland, et al., "Shear flow and drift wave turbulence dynamics in a cylindrical plasma device," Physics of Plasmas **17**, 032302 (2010).
[10]M. Xu, G. R. Tynan, C. Holland, et al., "Fourier-domain study of drift turbulence driven sheared flow in a laboratory plasma," Physics of Plasmas **17**, 032311 (2010).
[11]S. C. Thakur, C. Brandt, L. Cui, et al., "Multi-instability plasma dynamics during the route to fully developed turbulence in a helicon plasma," Plasma Sources Science and Technology **23**, 044006 (2014).
[12]L. Cui, G. R. Tynan, P. H. Diamond, et al., "Up-gradient particle flux in a drift wave-zonal flow system," Physics of Plasmas **22**, 050704 (2015).
[13]L. Cui, A. Ashourvan, S. C. Thakur, et al., "Spontaneous profile self-organization in a simple realization of drift-wave turbulence," Physics of Plasmas **23**, 055704 (2016).
[14]Y. Nagashima, S.-I. Itoh, S. Shinohara, et al., "Coexistence of zonal flows and drift-waves in a cylindrical magnetized plasma," Journal of the Physical Society of Japan **77**, 114501 (2008).
[15]Y. Nagashima, S.-I. Itoh, S. Shinohara, et al., "Observation of the parametric-modulational instability between the drift-wave fluctuation and azimuthally symmetric sheared radial electric field oscillation in a cylindrical laboratory plasma," Physics of Plasmas **16**, 020706 (2009).
[16]T. Yamada, S.-I. Itoh, T. Maruta, et al., "Experimental study of drift wave turbulence in linear plasmas," Plasma and Fusion Research **3**, 044–044 (2008).
[17]T. Yamada, S.-I. Itoh, S. Inagaki, et al., "Two-dimensional bispectral analysis of drift wave turbulence in a cylindrical plasma," Physics of Plasmas **17**, 052313 (2010).
[18]H. Arakawa, T. Kobayashi, S. Inagaki, et al., "Dynamic interaction between a solitary drift wave structure and zonal flows in a linear cylindrical device," Plasma Physics and Controlled Fusion **53**, 115009 (2011).
[19]S. Inagaki, T. Kobayashi, Y. Kosuga, et al., "A concept of cross-ferroic plasma turbulence," Scientific Reports **6**, 22189 (2016).
[20]R. J. Hajjar, P. H. Diamond, A. Ashourvan, and G. R. Tynan, "Modelling enhanced confinement in drift-wave turbulence," Physics of Plasmas **24**, 062106 (2017).
[21]R. J. Hajjar, P. H. Diamond, and G. R. Tynan, "The ecology of flows and drift wave turbulence in csdx: A model," Physics of Plasmas **25**, 022301 (2018).
[22]Y. KOSUGA, S.-I. ITOH, and K. ITOH, "Density peaking by parallel flow shear driven instability," Plasma and Fusion Research **10**, 3401024–3401024 (2015).
[23]M. Sasaki, N. Kasuya, K. Itoh, et al., "Topological bifurcation of helical flows in magnetized plasmas with density gradient and parallel flow shear," Physics of Plasmas **24**, 112103 (2017).
[24]N. Kasuya, S. Abe, M. Sasaki, et al., "Turbulence simulation taking account of inhomogeneity of neutral density in linear devices," Physics of Plasmas **25**, 012314 (2018).
[25]N. Kasuya and M. Sasaki, "Simulation research on competitive nature of plasma turbulence in linear devices," AIP Conference Proceedings **1993**, 020008 (2018).
[26]C. Y. Wang, W. W. Xiao, et al., "Intrinsic evolution on the decoupling-coupling-decoupling of the plasma density and temperature profiles in a cylindrical laboratory plasma device," submitted.
[27]W. W. Xiao, C. Y. Wang, J. X. Zhu, et al., AIP Advances **9**, 075026 (2019).
[28]P. Stangeby and G. McCracken, "Plasma boundary phenomena in tokamaks," Nuclear Fusion **30**, 005 (1990).
[29]P. C. Stangeby, "Plasma sheath transmission factors for tokamak edge plasmas," The Physics of Fluids **27**, 682–690 (1984).
[30]Y. C. Kim and E. J. Powers, "Digital bispectral analysis and its applications to nonlinear wave interactions," IEEE Transactions on Plasma Science **7**, 120–131 (1979).
[31]J. Cheng, J. Dong, K. Itoh, et al., "Lowintermediatehigh confinement transition in hl-2a tokamak plasmas," Nuclear Fusion **54**, 114004 (2014).
[32]Y. C. Kim and E. J. Powers, "Digital bispectral analysis of self-excited fluctuation spectra," Physics of Fluids **21**, 1452–1453 (1978).
[33]C. Ritz, D. Brower, T. Rhodes, et al., "Characterization of tokamak edge turbulence by far-infrared laser scattering and langmuir probes," Nuclear Fusion **27**, 1125–1134 (1987).
[34]P. H. Diamond, S.-I. Itoh, K. Itoh, and T. S. Hahm, "Zonal flows in plasma—a review," Plasma Physics and Controlled Fusion **47**, R35–R161 (2005).